第33卷第1期
2014年2月

红外与毫米波学报
J. Infrared Millim. Waves

Vol. 33, No. 1
February, 2014

文章编号：1001－9014(2014)01－0098－08

DOI：10.3724/SP.J.1010.2014.00098

A novel regularized adaptive edge-preserving image super-resolution algorithm

YU Hui[1,2], CHEN Fu-Sheng[2], ZHANG Zhi-Jie[2], WANG Chen-Sheng[2]

(1. School of Optical and Electronic Information, Huazhong University of Science and Technology, Hubei 430074, China;
2. Huazhong Institute of Electro-Optics-Wuhan National Lab for Optoelectronics, Hubei 430074, China)

Abstract: This paper proposed a novel adaptive regularization super-resolution (SR) method. The regularization term only penalizes the low-frequency components in the image. Meanwhile it protects the high-frequency components which may represent edge, in which the penalty threshold is automatically determined based on a linear function. For the selection of regularization parameter, a logarithmic function is proposed to adaptively determine the optimum regularization parameter in each iteration step instead of a constant regularization parameter. The proposed algorithm has been tested in the synthetic visiblelight image sequence and real infrared images. Experimental results show that the proposed approach is robust and can restore image details efficiently.

Key words: super-resolution; regularization term; regularization parameter; penalty threshold

PACS: 89.20.Ff

一种新的正规自适应边缘保护的超分辨率算法

余 徽[1,2], 陈福胜[2], 张智杰[2], 王晨晟[2]

(1. 华中科技大学 光学与电子信息学院,湖北 武汉 430074;
2. 华中光电技术研究所-武汉光电国家实验室,湖北 武汉 430074)

摘要: 主要提出了一个新的正规自适应超分辨率算法. 正规项只惩罚图像中可能包含有大量噪声的低频部分,同时保护图像中可能包含有锐利边缘的高频部分,其中,惩罚阈值自动地被一个线性函数决定. 对于正规参数的选择,这里不采用固定的正规参数而是提出一个对数函数在每次迭代时自适应地选择正规参数. 该算法经过仿真实验和真实的红外图像测试,实验结果显示该算法鲁棒性好,可以有效复原图像细节.

关 键 词: 超分辨率;正规项;正规参数;惩罚阈值

中图分类号: TP751.1 **文献标识码**: A

Introduction

Images with high resolution (HR) are often required in most electronic imaging application such as medical imaging[1], remote sensing[2]. In 1984, Tsai and Huang[3] first proposed super-resolution (SR) method which could obtain HR image from multiple low-resolution (LR) images based on frequency domain. For frequency domain-based method, the observation model is restricted to only global translational motion and linear space invariant (LSI) model, and the prior knowledge is difficult to be utilized. Therefore, various spatial domain-based methods have been proposed, such as maximum a posteriori (MAP) method[4], projection onto convex sets (POCS) approach[4], iterative back projection (IBP) algorithm[5], etc.

This paper is mainly based on the MAP model, in which both the regularization term and regularization parameter are very important elements. Generally, Gaussian smoothness prior is used to give the regulari-

Received date: 2012 - 10 - 13, **revised date**: 2013 - 04 - 18 **收稿日期**: 2012 - 10 - 13, **修回日期**: 2013 - 04 - 18

Biography: YU Hui (1989-), male, Wuhan Hubei province, China, PHD candidate. Research area involves infrared image registration, fusion and super-resolution reconstruction, E-mail: yuhuihust@gmail.com.

zation term in the MAP-based algorithm, but the reconstructed image may become over-smoothness. This paper mainly proposed a novel adaptively regularization method. The proposed regularization term only penalizes the small discontinuities in images which are usually caused by noise and protects the large discontinuities which are probably the edges. The penalty threshold is determined by an indirect parameter based on the rate of high-frequency component of the restored image. It is important to determine a suitable regularization parameter. If the parameter is too small the noise cannot be restrained efficiently. Conversely, the reconstructed image will be very blurry. Some methods have been proposed to determine the optimum regularization parameter directly. Vania[6] proposed a method based on a data-driven approach called generalized cross-validation. Bose[7] presented a method using L-Curve to select the regularization parameter. Dorota and Marek[8] selected the regularization parameter based on U-Curve. Although the methods presented above can provide good solutions the computational costs are very huge. In this paper, instead of selecting an optimum constant regularization parameter, an adaptive method adaptively choose the regularization parameter in each iteration step based on the ratio of fidelity term and regularization term.

The rest of the paper is organized as follows. Section 1 describes the image observation model. Section 2 describes the MAP-based model. The approaches to select the penalty threshold and regularization parameter are proposed in section 3. In section 4, the experimental results and analysis are presented.

1 Image Observation Model

This section describes a simple observation model. The original HR image with size of $l_1N_1 \times l_2N_2$ is denoted in lexicographical form as a vector $X = [x_1, x_2, \ldots x_n]$, where $n = l_1N_1l_2N_2$. Assume the observed LR image is obtained by warping, blurring, and downsampling the original HR image (Fig. 1) and the k-th observed LR image is denoted in lexicographical form as $y_k = [y_{k,1}, y_{k,2}, \ldots, y_{k,m}]$, where $k = 1, 2, \ldots p$ and m represents the size of LR image. The observation model can be formulated as:

$$y_k = DH_kM_kX + n_k \text{ for} k = 1,2,\ldots p \quad . \quad (1)$$

Let l_1 and l_2 present the down-sampled factors in vertical and horizontal directions respectively, and then the size of LR image represented by m is $N_1 \times N_2$. Matrix D of size $N_1N_2 \times l_1N_1l_2N_2$ represents the down-sampling process. H_k represents the blur matrix of size $l_1N_1l_2N_2 \times l_1N_1l_2N_2$. In this paper the blur matrix H_k is assumed to be the same for all observed LR images, so in the rest of this paper the blur matrix is represented by H. M_k stands for the warp matrix of size $l_1N_1l_2N_2 \times l_1N_1l_2N_2$; n_k represents the additional Gaussian noise of LR image which is denoted in a vector of size $N_1N_2 \times 1$.

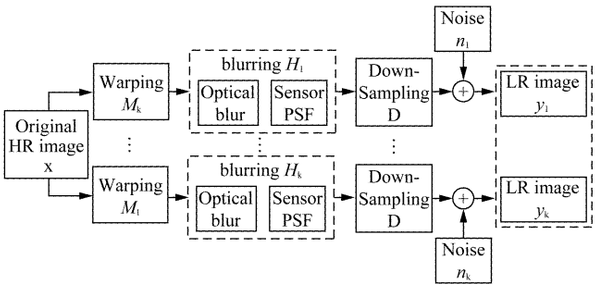

Fig. 1　Image observation model
图 1　图像观测模型

2 MAP-based SR Algorithm

Based on MAP model the estimated HR image from a sequence of LR images is given as:

$$\hat{X} = \arg\max \Pr(X \mid y_1, y_2, \ldots y_p) \quad . \quad (2)$$

Based on the Bayesian principle, equation (2) can be expressed as:

$$\hat{X} = \arg\max(\Pr(X)\ \Pr(y_1, y_2, \ldots y_p \mid X)) \quad , \quad (3)$$

where $\Pr(X)$ represents the image prior probability distribution, $\Pr(y_1, y_2, \ldots y_p \mid X)$ represents the conditional probability distribution of LR images. The conditional probability distribution of the LR image y_k is an independent noise probability density function. Then, the joint conditional probability density function of LR images is given as:

$$\Pr(y_1, y_2, \ldots y_p \mid X) = \left(\frac{1}{\sqrt{2\pi}\sigma_k}\right)^p \exp\left(-\sum_{k=1}^{p} \frac{\| y_k - DH_kM_kX \|^2}{2\sigma_k^2}\right) \quad , \quad (4)$$

where σ_k is the standard deviation of n_k. Based on

Markov random field (MRF) model[9], the probability density function of original image is given as:

$$\Pr(X) = \frac{1}{C}\exp\left\{-\frac{1}{2\beta}\sum_{c\in M}\rho_\alpha(L_cX)\right\} \quad , \quad (5)$$

$$\rho_\alpha(Z) = \sum_i \rho_\alpha(z_i) \quad . \quad (6)$$

In the equation (5), parameters C and β are constants. $\rho_\alpha(z)$ is the penalty function. In this paper, the penalty function is given as:

$$\rho_\alpha(z) = \begin{cases} z^2, & |z| \leqslant \alpha, \\ 0, & |z| > \alpha. \end{cases} \quad . \quad (7)$$

It can be seen that the proposed penalty function quadratically penalizes small discontinuities in images which are usually caused by noise and protects the large discontinuities which are probably the edges. Parameter α is the penalty threshold that separates the low-frequency and high-frequency. The second-order derivatives in four directions are applied as the image smooth measure. The kernels of the four operators $\{L_c\}_{c=1}^4$ are shown in Fig. 2.

1	-2	1

0	0	0.5
0	-1	0
0.5	0	0

1
-2
1

0.5	0	0
0	-1	0
0	0	0.5

Fig. 2 The mask of second-order derivative in four directions

图2 四个方向的二阶导数模板

Substituting equations (4) and (5) into (3), the SR reconstruction problem can be expressed as minimizing a cost function $E(X)$ given as:

$$\begin{aligned}\hat{X} &= \arg\min E(X) \\ &= \arg\min\Big(\sum_{k=1}^{p} \| y_k - DH_kM_kX \|^2 \\ &+ \lambda\sum_{c=1}^{4}\sum_{l=1}^{l_1N_1l_2N_2}\rho_\alpha([L_cX]_l)\Big) \quad . \quad (8)\end{aligned}$$

The first term of $E(X)$ represents the image fidelity, and the second term is regularization term stands for the image prior. λ is the regularization parameter which controls the trade-off between fidelity and prior knowledge. The second term of $E(X)$ can be simplified as:

$$\sum_{c=1}^{4}\sum_{l=1}^{l_1N_1l_2N_2}\rho_\alpha([L_cX]_l) = \sum_{c=1}^{4} XL_c^T\varphi_c(X)L_cX \quad , \quad (9)$$

where $\varphi_c(X)$ is a diagonal matrix with size $l_1N_1l_2N_2 \times l_1N_1l_1N_2$, and is given as:

$$[\varphi_c(X)]_{l,l} = \begin{cases} 1, & |[L_{cX}]|_l \leqslant \alpha, \\ 0, & otherwise. \end{cases} \quad . \quad (10)$$

Then, the estimated SR image can be given by:

$$\begin{aligned}\hat{X} &= \arg\min E(X) \\ &= \arg\min\Big(\sum_{k=1}^{p} \| y_k - DH_kM_kX \|^2 \\ &+ \lambda\sum_{c=1}^{4} XL_c^T\varphi_c(X)L_cX\Big) \quad . \quad (11)\end{aligned}$$

3 Parameter Determinations

In this section, the penalty threshold α and regularization parameter λ were determined and the Eq. (11) was solved by using gradient descent method.

3.1 Choice of Penalty Threshold

Based on Eq. (9), penalty function only quadratically penalizes the pixel whose second-order derivative is less than α. Initially, the amounts of high-frequency is very little, and then the initial value of α should be very large for the purpose of restraining the noise efficiently. With the progress of iteration, the high-frequency components of image are restored and the noise degree decreases, and the value of α should decrease with the iteration process to protect the edge from being blurry.

There are four high-pass filtering operators represented by $\{L_c\}_{c=1}^4$ operating on image $X^{(n)}$, and then four penalty thresholds denoted by $\{\alpha_c^{(n)}\}_{c=1}^4$ are updated in the n-th iteration step. Since it is difficult to determine the value of $\alpha_c^{(n)}$ directly, an indirect parameter $b^{(n)}$ is introduced. And then $\alpha_c^{(n)}$ is set based on the following equation:

$$\frac{N_{\alpha_c^{(n)}}(L_cX^{(n)})}{l_1Nl_1N_2} = b^{(n)} \quad , \quad (12)$$

where $N_{\alpha_c^{(n)}}(L_cX^{(n)})$ stands for the number of the non-zero value in diagonal matrix $\varphi_c(X^{(n)})$ when the penalty threshold is $\alpha_c^{(n)}$. When the value of $b^{(n)}$ is set as constant 1, the image prior is equivalent to Gaussian MRF prior. The parameter $b^{(n)}$ is set as a linear function of n, which is given as:

$$b^{(n)} = b^{(1)} - \eta(n-1) \quad , \quad (13)$$

where $b^{(1)}$ is the initial value set as 1. Parameter η stands for the step size set as 0.01 empirically. To pre-

vent the value of b from being too small, the value of b is set to be not less than 0.6 generally.

3.2 Choice of Regularization Parameter

Instead of determining a constant regularization parameter, this section proposed an iterative method that can adaptively estimate the regularization parameter based on the estimated HR image. The parameter λ is a function of X, and represented by $\lambda(X)$. $\lambda(X)$ should have the property that it can adaptively control the balance of the fidelity term $\sum_{k=1}^{p} \| y_k - DH_kM_kX \|^2$ and regularization term $\sum_{c=1}^{4} XL_c^T\varphi_c(X)L_cX$. When $\sum_{k=1}^{p} \| y_k - DH_kM_kX \|^2$ is large, $\lambda(X)$ should be larger so that the noise can be restrained efficiently. In the other hand, when $\sum_{c=1}^{4} XL_c^T\varphi_c(X)L_cX$ is large, $\lambda(X)$ should be smaller so that the high-frequency components of image can be protected. Motivated by the proposition above, an adaptive regularization parameter can be given by a logarithmic function:

$$\lambda(X) = A \cdot \ln\left(\frac{\sum_{k=1}^{p} \| y_k - DH_kM_kX \|^2}{\sum_{c=1}^{4} XL_c^T\varphi_c(X)L_cX} + 1\right). \quad (14)$$

The logarithmic function used here can avoid making regularization parameter too sensitive. Coefficient A is estimated by the following function:

$$\varepsilon = \frac{\sum_{i=1}^{N_1\times N_2} \left| \left[\left(\sum_{c=1}^{4} L_c y_k \right) \right]_i \right|}{N_1 \times N_2}, \quad (15)$$

where y_k represents any one of the LR images. Here, parameter ε can be described as the average of the second-order derivative of LR image pixel. Then coefficient A can be given by:

$$A = \frac{1}{\varepsilon} = \frac{N_1 \times N_2}{\sum_{i=1}^{N_1\times N_2} \left| \left[\left(\sum_{c=1}^{4} L_c y_k \right) \right]_i \right|}. \quad (16)$$

3.3 Gradient Descent Optimization

The procedures of gradient descent optimum are described as:

$$X^{(n+1)} = X^{(n)} - d^{(n)} \nabla_X E(X^{(n)}), \quad (17)$$

where $d^{(n)}$ represents the n-th iteration step size. $\nabla_X E(X)$ is approximately given as:

$$\begin{aligned} \nabla_X E(X) &= \nabla_X \left\{ \sum_{k=1}^{p} \| y_k - DH_kM_kX \|^2 + \lambda(X) \cdot \sum_{c=1}^{4} XL_c^T\varphi_c(X)L_cX \right\} \\ &\approx -2k \sum_{k=1}^{p} M_k^TH_k^TD^T(y_k - DH_kM_kX) + \lambda(X) \cdot \sum_{c=1}^{4} L_c^T\varphi_c(X)L_cX. \end{aligned} \quad (18)$$

Substituting equation (18) into equation (17), the iteration procedure is given as:

$$\begin{aligned} X^{(n+1)} = X^{(n)} - d^{(n)} \Big\{ & -2k \sum_{k=1}^{p} M_k^TH_k^TD^T(y_k - DH_kM_kX^{(n)}) \\ & + \lambda(X^{(n)}) \cdot \sum_{c=1}^{4} L_c^T\varphi_c(X)L_cX^{(n)} \Big\}, \end{aligned} \quad (19)$$

Step size $d^{(n)}$ should satisfy the following equation:

$$E(X^{(n)} - d^{(n)} \nabla E(X^{(n)})) = \min_{d\geq 0} E(X^{(n)} - d \nabla E(X^{(n)})), \quad (20)$$

Substituting equation (18) into (20), $d^{(n)}$ is given by:

$$d^{(n)} = \frac{\sum_{k=1}^{p} (\nabla E(X^{(n)}))^T M_k^TH_k^TD^T(DH_kM_kX^{(n)} - y_k) + \lambda(X^{(n)})(\nabla E(X^{(n)}))^T (\sum_{c=1}^{4} L_c^T\varphi_c(X^{(n)})L_c)X^{(n)}}{(\nabla E(X^{(n)}))^T (\sum_{c=1}^{4} L_c^T\varphi_c(X^{(n)})L_c) \nabla E(X^{(n)}) + \sum_{k=1}^{p} \| DH_kM_k \nabla E(X^{(n)}) \|^2}, \quad (21)$$

4 Experiments

4.1 Simulation experiments

The simulated image sequences were obtained by translating, blurring, and down-sampling the original HR images including: "Airfield" of size 256×256 and "Bridge" of size 240×240, shown in Fig. 4(a) and Fig. 6(a). First, original HR images were translated with different horizontal shift and vertical shift to produce four images. The process of blurring was simulated by applying PSF of 5×5 window size and 0.5 variance. Then the blurred images were down-sampled with a factor of 2. Lastly, zero-mean Gaussian noise with three different power 10 dB, 15 dB and 20 dB was added to the down-sampled images. The initialization of X was given by the Bilinear interpolation (BI) method. The structural similarity (SSIM) and peak signal to noise ratio (PSNR) were used to evaluate the objective quality of reconstructed SR images.

To verify the efficiency of the proposed method, it

was compared with constant parameter method and Gaussian MRF-based method[4] represented by algorithm I and algorithm II, respectively. Because it is difficult to obtain the optimum constant parameters, two sequences of constants λ and constants b have been tested in the case of noise power 10 dB as shown in Fig. 3. The results show that for "Airfield" image the optimum values of parameter λ and parameter b are 0.1 and 0.7 respectively, and for "bridge" image they are 0.075 and 0.7 respectively. The values of PSNR and SSIM are shown in Table 1. From Table 1, it is observed that the proposed method can obtain better results than the others. The reconstructed images obtained with different methods in the case of noise power 10 dB are shown in Fig. 4 and Fig. 6. The detailed images of the results are shown in Fig. 5 and Fig. 7. The results show that the proposed method can restore more details than the constant parameter method and Gaussian MRF-based method.

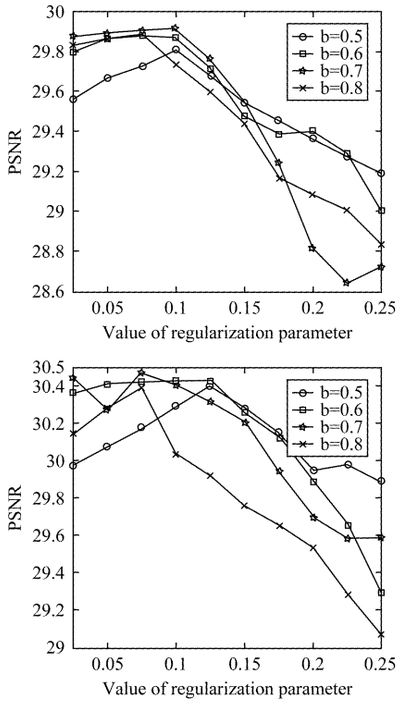

Fig. 3 PSNR versus the constant regularization parameter for "airfield" image (left) and "bridge" image (right) in the case of noise power 10 dB
图3 在噪声功率10 dB情况下"airfield"(左)和"bridge"(右)的PSNR值与固定参数的关系曲线

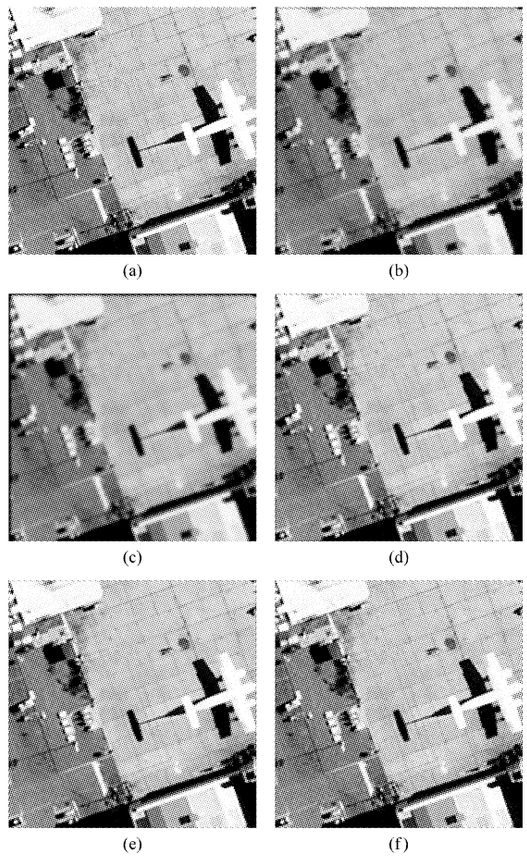

Fig. 4 In the case of noise power 10 dB, SR reconstruction results of the "airfield" image: (a) Original image; (b) LR image; (c) BI; (d) Algorithm Ⅱ; (e) Algorithm Ⅰ; (f) Proposed algorithm
图4 噪声功率10 dB时,"airfield"图像的SR重建结果:(a)原始图像;(b)低分辨率图像;(c)双线性插值法;(d)算法Ⅱ;(e)算法Ⅰ;(f)本文提出的算法

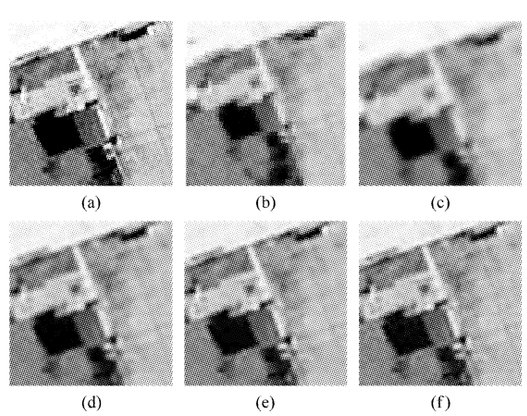

Fig. 5 Partially magnified images shown in Fig. 4: (a) Original image; (b) LR image; (c) BI; (d) Algorithm Ⅱ; (e) Algorithm Ⅰ; (f) Proposed algorithm
图5 图4中的部分放大图像:(a)原始图像;(b)低分辨率图像;(c)双线性插值法;(d)算法Ⅱ;(e)算法Ⅰ;(f)本文提出的算法

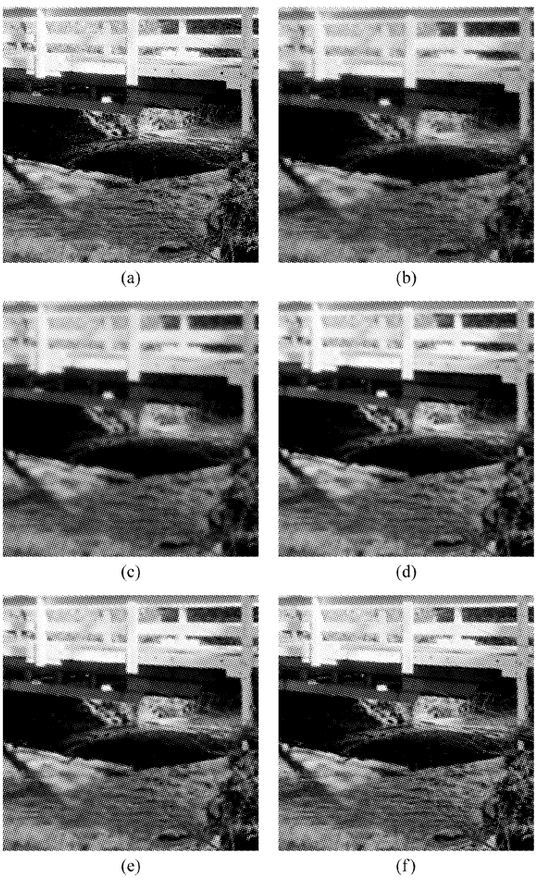

Fig. 6　In the case of noise power 10 dB, SR reconstruction results of the "bridge" image: (a) Original image; (b) LR image; (c) BI; (d) Algorithm Ⅱ; (e) Algorithm Ⅰ; (f) Proposed algorithm
图 6　噪声功率 10 dB 时, "bridge"图像的 SR 重建结果: (a)原始图像;(b)低分辨率图像;(c)双线性插值法;(d)算法Ⅱ;(e)算法Ⅰ;(f)本文提出的算法

The values of regularization parameter versus iteration numbers are shown in Fig. 8. It is observed that the regularization parameter decreases with the progress of iteration. When the degree of noise power is higher, the regularization function adaptively selected the larger value to restrict the noise efficiently. Conversely, when the power of noise gets lower, the regularization function selected the lower value to preserve the image details. The fidelity term and regularization term normalized by the number of pixels are shown in Fig. 9. Only the results from "airfield" are given since the results from "bridge" are similar to those from "airfield". Figure 9 shows that the value of $\sum_{k=1}^{p} \| y_k - DH_kM_kX \|^2$ decreases with the progress

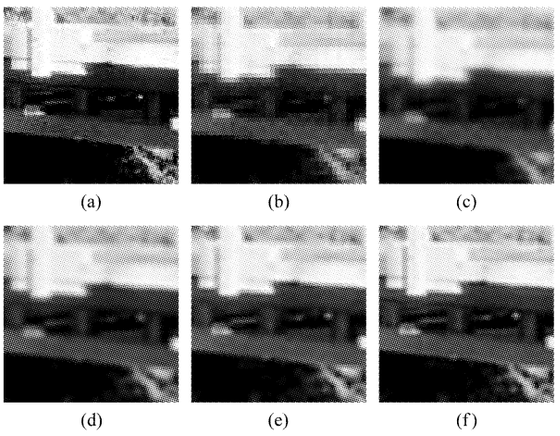

Fig. 7　Partially magnified images shown in Fig. 6: (a) Original image; (b) LR image; (c) BI; (d) Algorithm Ⅱ; (e) Algorithm Ⅰ; (f) Proposed algorithm
图 7　图 6 中的部分放大图像: (a)原始图像;(b)低分辨率图像;(c)双线性插值法;(d)算法Ⅱ;(e)算法Ⅰ;(f)本文提出的算法

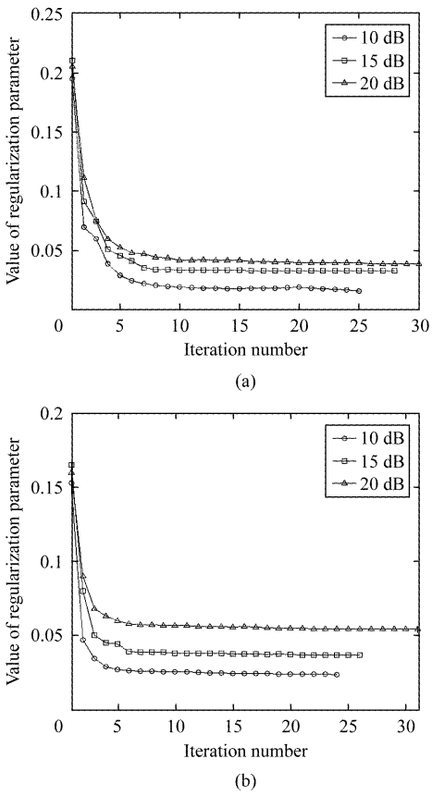

Fig. 8　In the cases of different noise power, the value of regularization parameter $\lambda^{(n)}$ versus iteration number for case of simulation experiments. (a) airfield; (b) bridge
图 8　在不同噪声功率情况下正规参数值与迭代次数的关系曲线. (a) airfield; (b) bridge

of iteration and converges to a value close to the power of noise. Then, as a by-product, the noise power can be estimated by the proposed algorithm without any prior information.

The number of terminative iteration for different algorithm is shown in Table 2. It can be seen that the number of iteration for using the proposed method is the largest one which means that the proposed algorithm preserves edge better at the cost of time-consuming. Though the number of iteration for using fixed regularization parameter is less than that for using proposed method, the optimum regularization parameter is obtained by testing a sequence of candidate values, and it may cost more time.

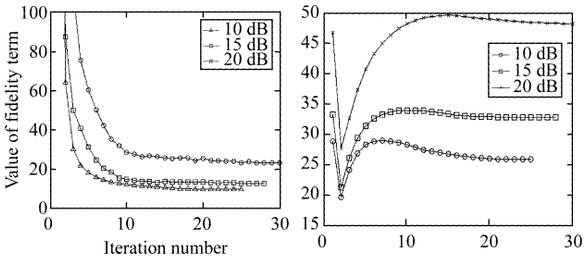

Fig. 9 For image "airfield" the values of fidelity term (left) and prior term (right) versus the iteration number in the cases of different noise power
图9 "airfield"不同噪声下保真项(左)和正规项(右)的值与迭代次数的关系曲线

Table 1 Values of PSNR and SSIM by using different algorithm
表1 不同算法重建结果的 PSNR 值和 SSIM 值

		BI	Algorithm Ⅱ	Algorithm Ⅰ	Proposed algorithm
10 dB					
PSNR	Airfield	17.7146	28.9642	29.9150	29.9246
	Bridge	18.8218	29.2947	30.4418	30.5756
SSIM	Airfield	0.7906	0.9032	0.9184	0.929
	Bridge	0.8015	0.9081	0.9198	0.9315
15 dB					
PSNR	Airfield	17.6829	27.2827	28.3679	28.7946
	Bridge	18.7624	28.1513	28.3944	28.9143
SSIM	Airfield	0.7851	0.8977	0.9088	0.9172
	Bridge	0.7964	0.8985	0.9083	0.9217
20 dB					
PSNR	Airfield	17.5374	26.5237	26.6914	27.3587
	Bridge	18.6307	26.4182	26.7786	27.6217
SSIM	Airfield	0.7829	0.8804	0.8825	0.8933
	Bridge	0.7953	0.8812	0.8819	0.8942

Table 2 Number of terminative iteration from different algorithms
表2 不同算法的迭代次数

		Algorithm Ⅱ	Algorithm Ⅰ	Proposed algorithm
10 dB	Airfield	17	20	25
	Bridge	19	24	24
15 dB	Airfield	18	23	28
	Bridge	21	26	26
20 dB	Airfield	22	26	30
	Bridge	25	28	31

4.2 Real experiments

In this section, the proposed algorithm was tested on the real infrared image sequences of size 240 × 240 obtained by the infrared thermal imaging which has the micro-scan architecture that can obtain the image with subpixel motion of 0.5 pixel. For the case of using algorithm Ⅰ, the optimum values of b and λ are set as 0.7 and 0.1 respectively based on the simulation results. The SR reconstructed images from different algorithms are shown in Fig. 10 and the detailed images of the results are shown in Fig. 11. From the results it is observed that the proposed method can restore more image details than other methods.

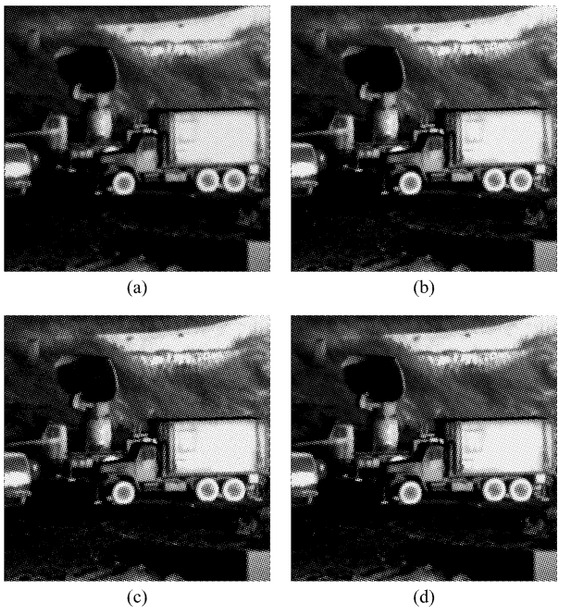

Fig. 10 SR reconstruction results of "vehicle": (a) BI; (b) Algorithm Ⅱ; (c) Algorithm Ⅰ; (d) Proposed algorithm
图10 "vehicle"图像的 SR 重建结果:(a) 双线性插值法;(b) 算法Ⅱ;(c) 算法Ⅰ;(d) 本文提出的算法

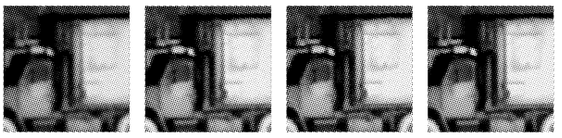

(a)　(b)　(c)　(d)

Fig. 11　Partially magnified images shown in Fig. 11: (a) BI; (b) Algorithm Ⅱ; (c) Algorithm Ⅰ; (d) Proposed algorithm

图 11　图 10 中的部分放大图像: (a) 双线性插值法; (b) 算法Ⅱ; (c) 算法Ⅰ; (d) 本文提出的算法

5　Conclusions

In this paper, a novel adaptive regularization method was proposed. The regularization term only penalizes the low-frequency components and protects the high-frequency which may represent edge. The penalty threshold is determined by a linear function. The regularization parameter is adaptively selected by a logarithmic function based on the ratio of fidelity term and regularization term. The experimental results show that the proposed method can preserve the edge well and obtain better results than the Gaussian MRF-based method and constant parameter method in both quantitative term and visual effects.

REFERENCES

[1] Wallach D, Lamare F, Roux C, *et al*. Biomedical Imaging: From Nano to Macro, [J]. *IEEE International Symposium on*, **2009**: 931 - 934.

[2] Chan J-W, Ma J, Kempeneers P, *et al*. Superresolution enhancement of hyperspectral CHRIS/Proba images with a thin-plate spline nonrigid transform model [J]. *Geoscience and Remote Sensing, IEEE Transactions on*, 2010, **48**(6): 2569 - 2579.

[3] Huang T S, Tsay R Y. Advances in Computer Vision and Image Processing, [J]. 1984, **1**(2): 317 - 339.

[4] Park S C, Park M K, Kang M G. Super-resolution image reconstruction: a technical overview [J]. *Signal Processing Magazine, IEEE*, 2003, **20**(3): 21 - 36.

[5] Qin F-q, He X-h, Chen W-l, *et al*. Video superresolution reconstruction based on subpixel registration and iterative back projection [J]. *Journal of Electronic Imaging*, 2009, **18**(1): 013007 - 013007 - 013011.

[6] Estrela V V, Galatsanos N P. Image Processing, 1998. ICIP 98. Proceedings [C]. 1998 *International Conference on*, 1998, **2**: 200 - 203.

[7] Bose N K, Lertrattanapanich S, Koo J. Circuits and Systems, 2001. ISCAS 2001 [C]. *The* 2001 *IEEE International Symposium on*, 2001, **2**: 433 - 436.

[8] Krawczyk-StańDo D, Rudnicki M. Regularization parameter selection in discrete ill-posed problems—the use of the U-curve [J]. *International Journal of Applied Mathematics and Computer Science*, 2007, **17**(2): 157 - 164.

[9] Panagiotopoulou A, Anastassopoulos V. Regularized super-resolution image reconstruction employing robust error norms [J]. *Optical Engineering*, 2009, **48**(11): 117004 - 117004 - 117014.

(上接 61 页)

[14] YUAN Xue-Song, LAN Ying, MA Chun-Yan, *et al*. Theoretical study on a 0.6 THz third harmonic gyrotron, *Phys. Plasmas* [J], 2011, **18**: 103115.

[15] GENG Zhi-Hui, LIU Pu-Kun, SU Yi-Nong, *et al*. Design of a Ka band 35 kW CW low-voltage harmonic gyrotron [J], *Int J. Infrared Millim. Waves*, 2010, **31**(1): 41 - 47.

[16] CAO Xiao-Qin, LIU Pu-Kun. Self-consistend nonlinear computation of a 28 GHzV gyrotron at the second harmonic. [J]. *J. Infrared Millim. Waves* (曹晓琴, 刘濮鲲. 28 GHzV二次谐波回旋振荡管的自洽非线性计算. **红外与毫米波学报**)2005, **24**(4): 317 - 320.

[17] YUAN Xue-Song, YAN Yang, FU Wen-Jie, *et al*. Multimode high harmonic operation in a terahertz gyrotron. [J]. *J. Jnfrared Millim. Waves* (袁学松, 鄢扬, 傅文杰, 等, 高次谐波太赫兹回旋管的多模工作. **红外与毫米波学报**)2012, **31**(4): 342 - 347.

[18] Huang Yong, Li Hongfu, Du Pingzhong, *et al*. Third-harmonic complex cavity gyrotron self-consistent nonlinear analysis, *IEEE Trans. Plasma Sci* [J]. 1997, **25**(6): 1406 - 1411.

[19] Du Chao-Hai, Liu Pu-Kun . Beam-wave coupling strength analysis in a gyrotron traveling-wave amplifier, *J Infrared Milli Terahz Waves* [J]. 2010, **31**: 714 - 723.

[20] Liu P-K, Borie E, Kartikeyan M V. Design of a 24 GHzV, 25-50 kW technology gyrotron operating at the second harmonic, Int. *J. Infrared and Millimeter Waves* [J]. 2000, **21**(12): 1917 - 1943.

[21] Fliflet A W, Read M E, Chu K R, *et al*. A self- consistent field theory for gyrotron oscillator: application to a low Q gyromonotron, Int. *J. Electronics* [J]. 1983, **53**(6): 505 - 521.

[22] Chu K R. Theory of electron cyclotron maser interaction in a cavity at the harmonic frequencies, *Phys. Fluids* [J]. 1978, **21**(12): 2354 - 2364.